JMEPEG (1994) 3:371-377

Comparison of Corrosion-Fatigue Properties of Precorroded 6013 Bare and 2024 Bare Aluminum Alloy Sheet Materials

J. Chaudhuri, Y.M. Tan, V. Gondhalekar, and K.M. Patni

The corrosion-fatigue resistance of precorroded 6013 bare and 2024 bare aluminum alloy sheet materials was evaluated to compare the effect of corrosion on initiation and propagation of fatigue cracks. The specimens were precorroded in 3.5% NaCl water solution per ASTM G 44 for periods of 4 and 30 days, and then were subjected to cyclic testing to failure in a 3.5% NaCl corrosive environment. The notched 6013 specimens showed better corrosion-fatigue resistance for the longer exposure time only. In all other cases, the 2024 material had better resistance. Fractographic and microstructural examinations suggested that the lower corrosion-fatigue life of the 6013 alloy is due to intergranular corrosion. Although the surface corrosion (pitting) on the 2024 alloy appeared severe, there was little evidence of intergranular corrosion in this alloy.

Keywords

aluminum alloys, corrosion-fatigue, 2024 aluminum alloy, 6013 aluminum alloy

1. Introduction

The increasing use of 6013 aluminum alloy (Al-0.8Si-0.9Cu-0.95Mg-0.35Mn) sheet material in new aircraft designs can be attributed to these beneficial properties:

- Good stretch-forming characteristics in the T4 temper (solution heat treated and naturally aged to a substantially stable condition), comparable to those of 2024 alloy (Al-4.4Cu-0.6Mn-1.5Mg) in the W temper (solution heat treated; applicable only to alloys that spontaneously age at room temperature). This property helps to reduce fabrication costs.
- Finer grain size than conventional aluminum sheet materials such as 2024, which minimizes the occurrence of the "orange peel" condition during stretch-forming operations
- Weldability comparable to that of 6061 alloy
- Cost comparable to that of 2024-T3 sheet material
- Higher tensile and compressive yield strengths and 3% lower density than 2024 alloy
- 25% higher strength than 6061 alloy
- Fatigue properties and fracture toughness comparable to those of Alclad 2024

Potential applications of this material include structural parts, such as wing and fuselage skins traditionally fabricated from Alclad 2024 and 2024 bare sheet materials (2024 bare is used specifically in the bonded joints in the aircraft structure). Based on earlier data, it can be concluded that the dry-air fatigue life of 6013 alloy is comparable to that of 2024 alloy (Ref 1, 2). Earlier investigation of the corrosion-fatigue properties of 6013-T6 alloy concluded that it has slightly lower corrosion-fatigue life compared to 2024-T3 bare and much lower corrosion-fatigue life than Alclad 2024-T3 (Ref 3). The reduced life of 6013-T6 bare can be attributed to observed intergranular corrosion (Ref 3-5). Despite its intergranular susceptibility, 6013-T6 alloy is highly resistant to stress-corrosion cracking and exfoliation corrosion. In order to obtain a more realistic evaluation, a useful investigation would be to separate the effect of corrosion on the initiation and propagation of fatigue cracks. Hence, we decided to perform the corrosion-fatigue test (Ref 6) on precorroded specimens.

J. Chaudhuri and **Y.M. Tan,** Mechanical Engineering Department, Wichita State University, Wichita, KS 67260-0035, USA; **V. Gondhalekar** and **K. Patni,** Materials and Processes Division, Cessna Aircraft Company, Wichita, KS, 67277, USA

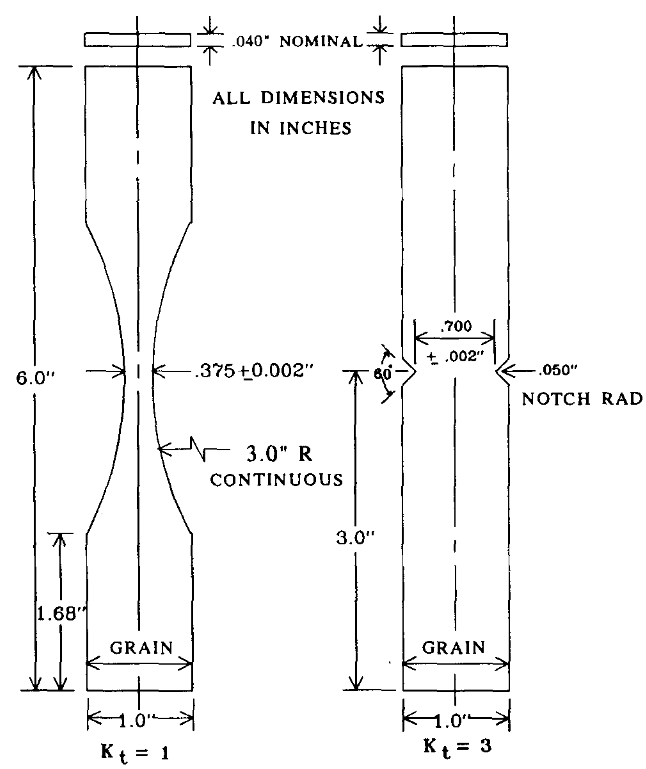

Fig. 1 Test specimen geometry (1" = 2.54 cm).

2. Experimental Work

Test specimens were fabricated per ASTM E 466 from 1 mm (0.04 in.) thick 6013-T6 bare and 2024-T3 bare sheet materials. The test specimen geometries were as shown in Fig. 1 for stress-concentration factors of $K_t = 1$ and $K_t = 3$. Specimens were precorroded in 3.5% salt water per ASTM G 44 for periods of 4 and 30 days to develop corrosion pits for the initiation and propagation of cracks. The grip sections of the specimens were masked during precorrosion.

Details of the corrosion-fatigue test procedure are given in Ref 7. Constant-amplitude, sinusoidal-loading corrosion-fatigue tests were conducted on the precorroded specimens by placing a corrosion cell around the test specimen gage area (Fig. 2). A uniform, linear flow of 3.5% aerated salt water, per ASTM G 44, was maintained through the corrosion cell at a flow rate of 0.6 to 0.8 L/min (10 to 12 gal/h), and the water line was kept at the center of the specimen gage-section area. The maximum stress levels were selected from previous data on corrosion-fatigue testing of these alloys without precorrosion (Ref 3) and are listed in Table 1. The stress ratio between the maximum and minimum fatigue cycling load was 0.1, and a frequency of 0.5 Hz was used. Each test was repeated three times. All specimens were subjected to corrosion-fatigue testing to failure by fracture (i.e., separation of the specimen into two pieces).

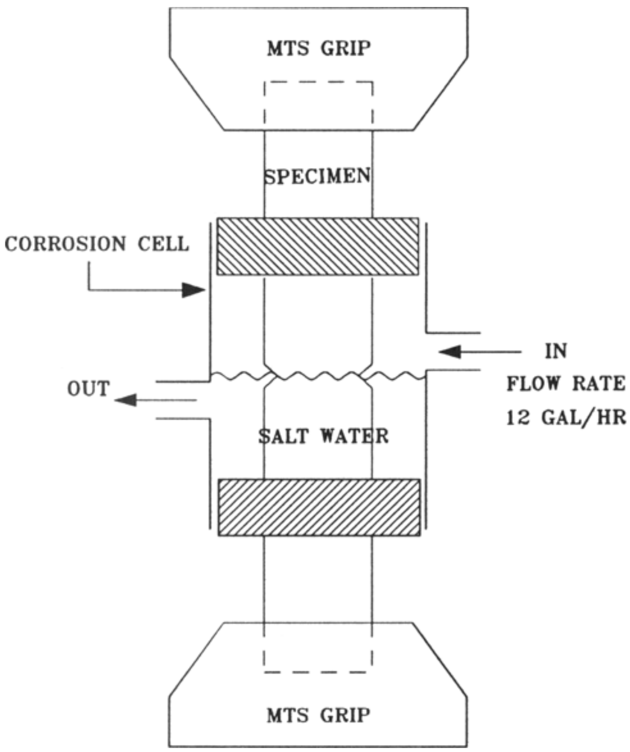

Fig. 2 Corrosion cell setup

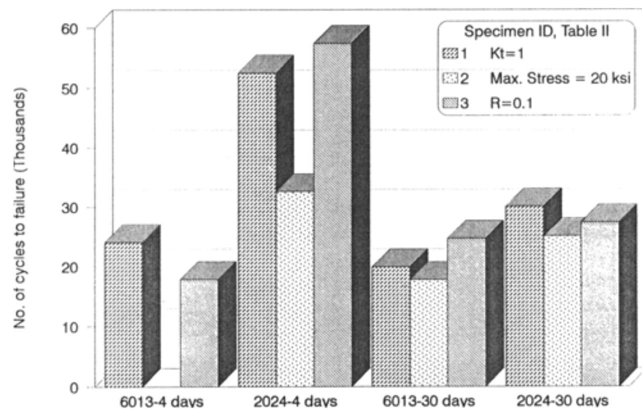

Fig. 3 Corrosion-fatigue life at a maximum stress of 140 MPa (20 ksi), $K_t = 1$, and precorrosion periods of 4 and 30 days

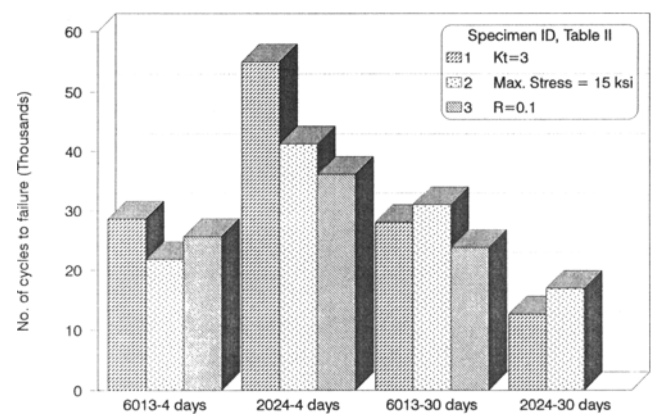

Fig. 4 Corrosion-fatigue life at a maximum stress of 105 MPa (15 ksi), $K_t = 3$, and precorrosion periods of 4 and 30 days

Table 1 Cyclic test specimen matrix

Alloy	Maximum stress, MPa	Maximum stress, ksi	Stress-concentration factor (K_t)	Length of precorrosion, days	No. of tests
6013-T6	140	20	1	4	3
	105	15	3	4	3
2024-T3	140	20	1	4	3
	105	15	3	4	3
6013-T6	140	20	1	30	3
	105	15	3	30	3
2024-T3	140	20	1	30	3
	105	15	3	30	3

Note: A total of 24 specimens were tested.

3. Results and Discussion

3.1 *Corrosion-Fatigue Test Results*

The corrosion-fatigue test data for the precorroded specimens are listed in Table 2 and shown in Fig. 3 to 6. On average, compared to the 2024 bare alloy, for $K_t = 1$ and a stress level of 140 MPa (20 ksi), the 6013 bare alloy showed a reduction in corrosion-fatigue life by 56% for 4 days of precorrosion and by 24% for 30 days of precorrosion. For $K_t = 3$ and a stress level of 105 MPa (15 ksi), the corrosion-fatigue life of the 6013 bare alloy was reduced by 42% for 4 days of precorrosion, but increased by 87% for 30 days of precorrosion when compared to the 2024 bare alloy. For comparison, Fig. 5 and 6 also contain corrosion-fatigue data for 2024 bare and 6013 bare alloys without precorrosion (Ref 3).

3.2 *Visual Examination*

All the specimens were visually examined after precorrosion to investigate the extent of corrosion on the surface. Surface corrosion in the 2024 bare alloy was clearly visible, and severity increased with exposure time (Fig. 7 and 8). On the other hand, surface corrosion in the 6013 bare alloy was not clearly visible, and severity increased only moderately with exposure time (Fig. 9 and 10). It should be pointed out that be-

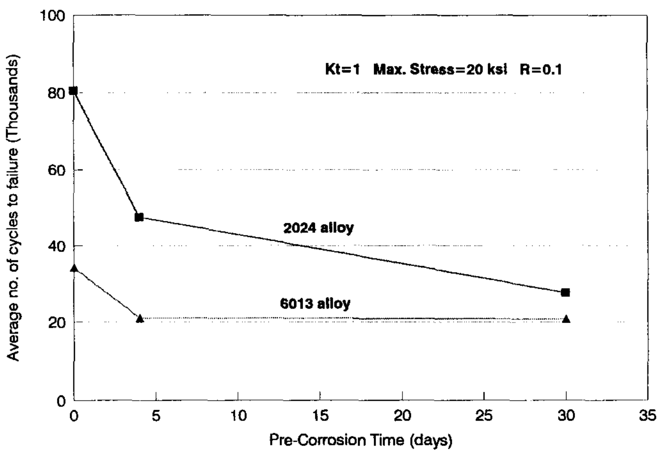

Fig. 5 Average number of cycles to failure versus length of precorrosion at a maximum stress of 140 MPa (20 ksi) and $K_t = 1$

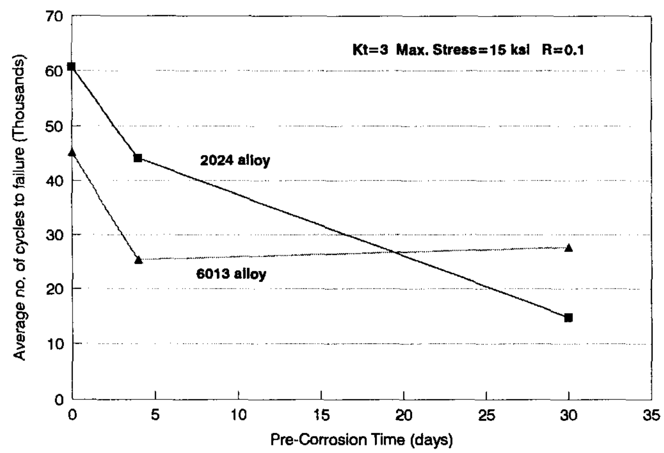

Fig. 6 Average number of cycles to failure versus length of precorrosion at a maximum stress of 105 MPa (15 ksi) and $K_t = 3$

Table 2 Corrosion-fatigue test results

Alloy	Sample No.	Length of precorrosion, days	Maximum stress MPa	Maximum stress ksi	Stress-concentration factor (K_t)	Number of cycles to failure	Average number of Cycles to failure
6013-T6	1	4	140	20	1	24,139	21,015
	2	4	140	20	1	48,145(a)(b)	
	3	4	140	20	1	17,891	
2024-T3	1	4	140	20	1	52,459	47,499
	2	4	140	20	1	32,614	
	3	4	140	20	1	57,423	
6013-T6	1	30	140	20	1	19,960	20,830
	2	30	140	20	1	17,800	
	3	30	140	20	1	24,731	
2024-T3	1	30	140	20	1	30,138	27,573
	2	30	140	20	1	25,151	
	3	30	140	20	1	27,431	
6013-T6	1	4	105	15	3	28,647	25,386
	2	4	105	15	3	21,821	
	3	4	105	15	3	25,690	
2024-T3	1	4	105	15	3	54,954	44,150
	2	4	105	15	3	41,300	
	3	4	105	15	3	36,197	
6013-T6	1	30	105	15	3	28,059	27,634
	2	30	105	15	3	31,029	
	3	30	105	15	3	23,814	
2024-T3	1	30	105	15	3	12,625	14,791
	2	30	105	15	3	16,956	
	3	30	105	15	3	>30,000(b)(c)	

(a) The water pump stopped running during the test. (b) The average was calculated without considering the number of cycles to failure for that specimen. (c) The test was halted because the water pump had stopped running.

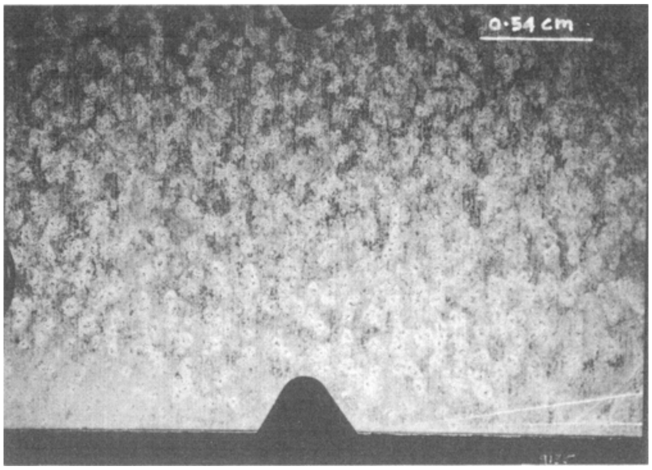

Fig. 7 Typical photograph of a 2024 bare specimen at $K_t = 3$ and 4 days of precorrosion

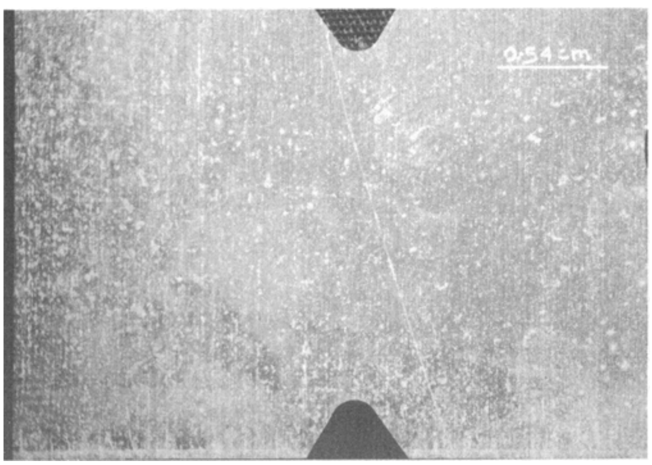

Fig. 8 Typical photograph of a 2024 bare specimen at $K_t = 3$ and 30 days of precorrosion

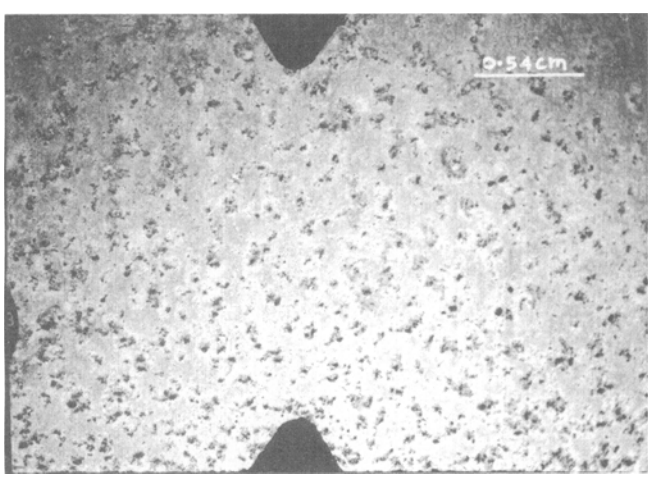

Fig. 9 Typical photograph of a 6013 bare specimen at $K_t = 3$ and 4 days of precorrosion

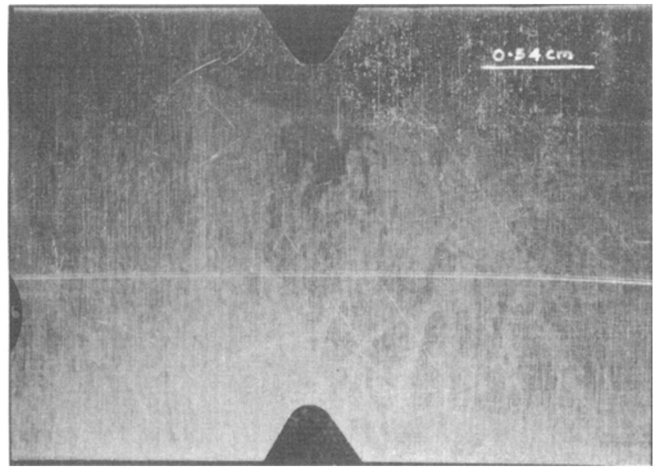

Fig. 10 Typical photograph of a 6013 bare specimen at $K_t = 3$ and 30 days of precorrosion

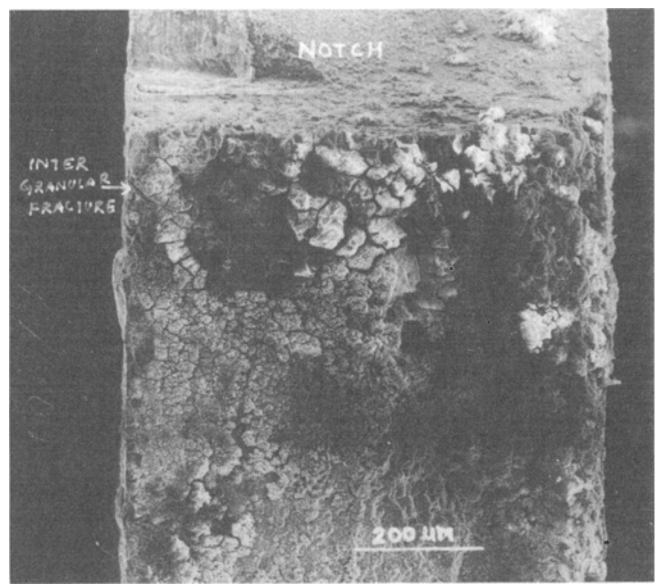

Fig. 11 Scanning electron micrograph near the notch of the 6013 fracture specimen ($K_t = 3$ and 4 days of precorrosion) showing intergranular cracking. The corrosion was so intense that it destroyed the fatigue features.

cause the surface corrosion in the 2024 bare alloy was visible, it could readily be inspected; the surface corrosion in the 6013 bare alloy was not easily visible and thus was difficult to inspect.

3.3 *Fractographic Examination*

The notched specimens with the shortest corrosion-fatigue life in each group were examined using scanning electron microscopy. Figures 11 and 12 show that the 6013 bare alloy specimen with $K_t = 3$ and 4 days of precorrosion exhibited intergranular corrosion with both primary and secondary cracking. The severity of the corrosion destroyed the fatigue features. In addition, corrosion pits were observed both at the

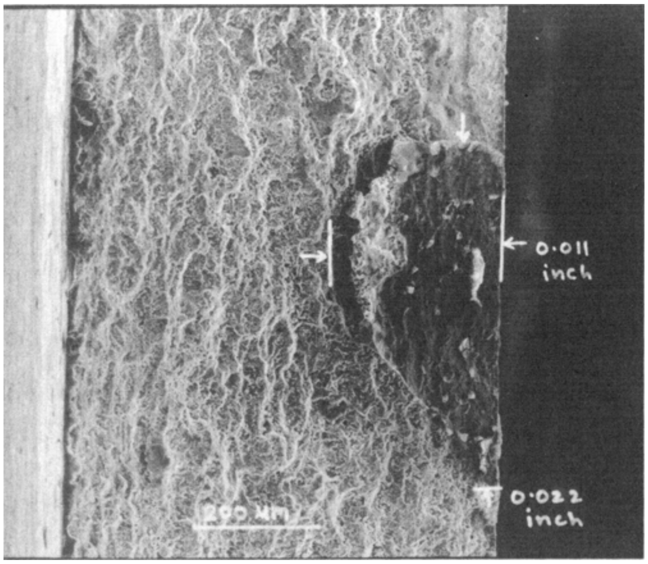

Fig. 12 Scanning electron micrograph of the fracture surface of the same specimen in Fig. 11, showing secondary cracking

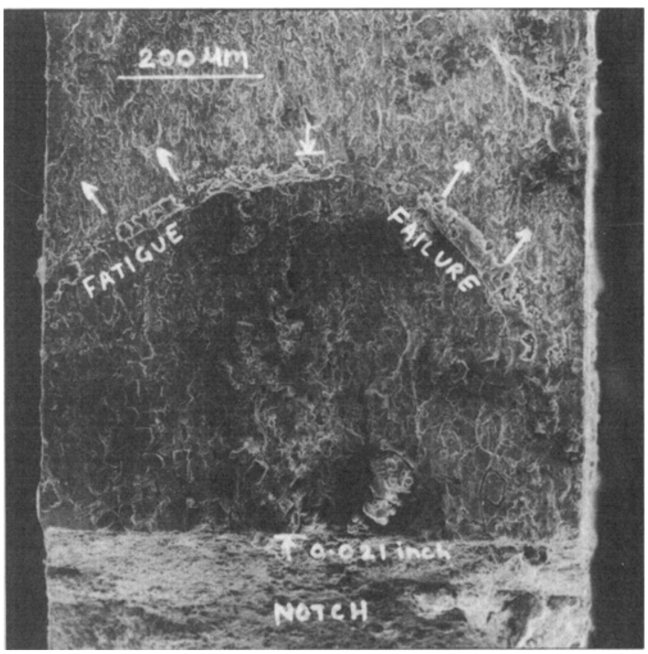

Fig. 13 Scanning electron micrograph of the 2024 fracture specimen (K_t = 3 and 4 days of precorrosion) showing corrosion fatigue failure

fracture surface edge and at the notch. The 2024 bare alloy specimen indicated corrosion-fatigue features only close to the notch. The specimen surface showed some secondary corrosion-fatigue damage (Fig. 13 and 14).

Microscopic examination of the fracture specimens with K_t = 3 and 30 days of precorrosion primarily revealed similar features, but the severity of the corrosion increased. Intergranular primary cracking at the tip of the notch was observed in the 6013 bare alloy specimen with K_t = 3 and 30 days of exposure (Fig. 15 to 17). Corrosion pits were observed at the notch as

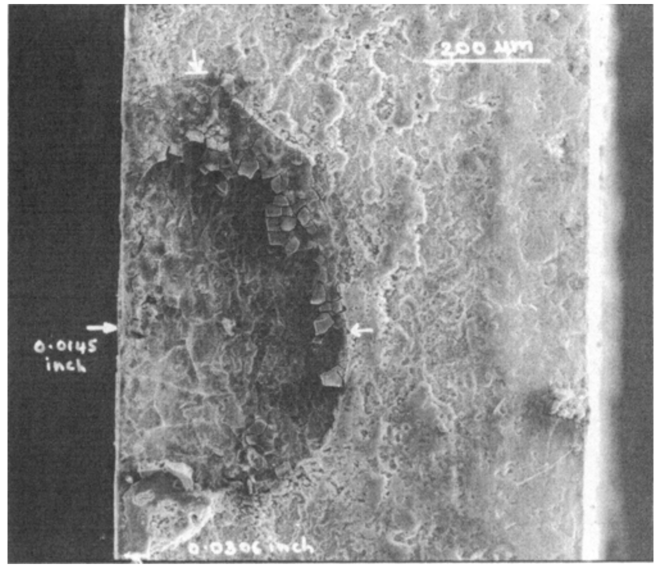

Fig. 14 Scanning electron micrograph of the fracture surface of the same specimen in Fig. 13, showing secondary corrosion-fatigue damage

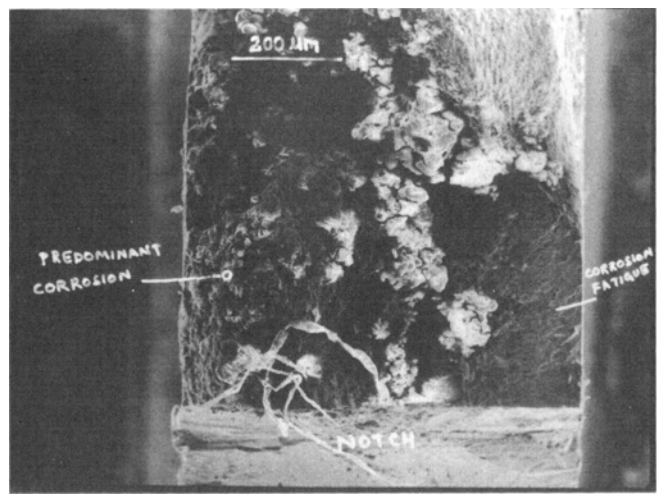

Fig. 15 Scanning electron micrograph of the 6013 bare fracture specimen (K_t = 3 and 30 days of precorrosion) showing the heavily corroded crack origin area near the notch

well as on the fracture surface edge. The 2024 bare alloy specimen with K_t = 3 and 30 days of exposure showed heavy corrosion pitting both at the notch and at the surface (Fig. 18 and 19). Fatigue initiation occurred from these corrosion sites.

3.4 *Metallographic Examination*

Microstructural examination using an optical microscope was performed on the same specimens used for the fractographic examination. The specimens were cross-sectioned at the location of maximum corrosion damage as indicated by visual examination, and metallurgical mounts were prepared. The 6013 bare alloy specimen with K_t = 3 and 4 days of precorrosion showed intergranular cracking at the fracture surface

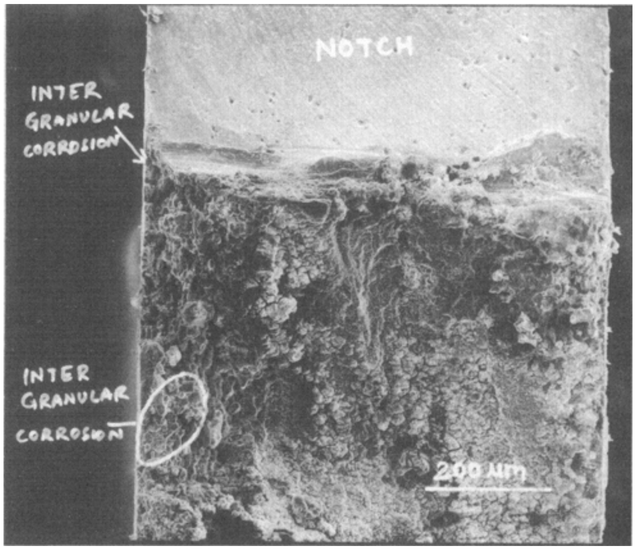

Fig. 16 Scanning electron micrograph of the area opposite the crack origin area shown in Fig. 15, indicating intensive intergranular fracture

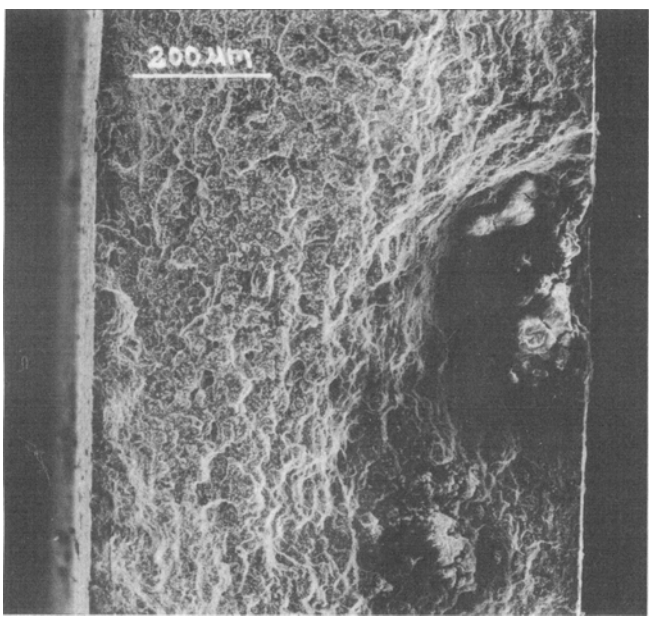

Fig. 17 Scanning electron micrograph of the same specimen in Fig. 15, showing secondary intergranular corrosion on the specimen surface

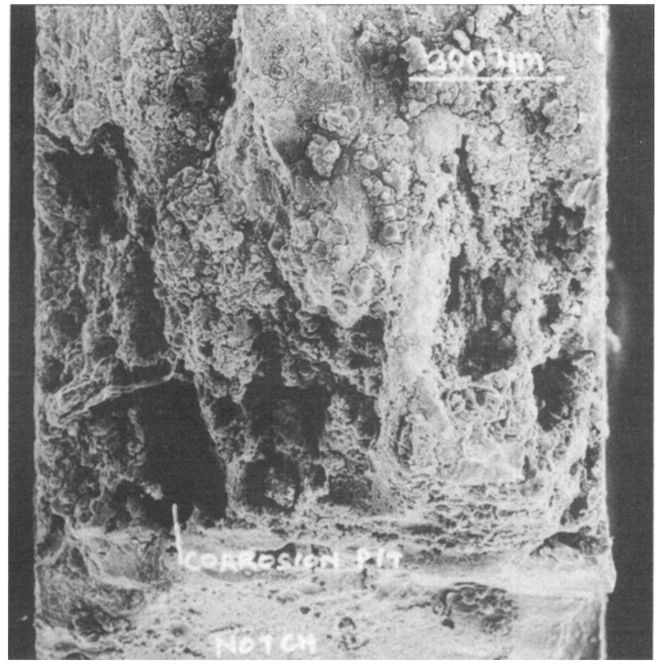

Fig. 18 Scanning electron micrograph of the fracture surface of the 2024 bare specimen ($K_t = 3$ and 30 days of precorrosion) at the notch, showing corrosion pitting

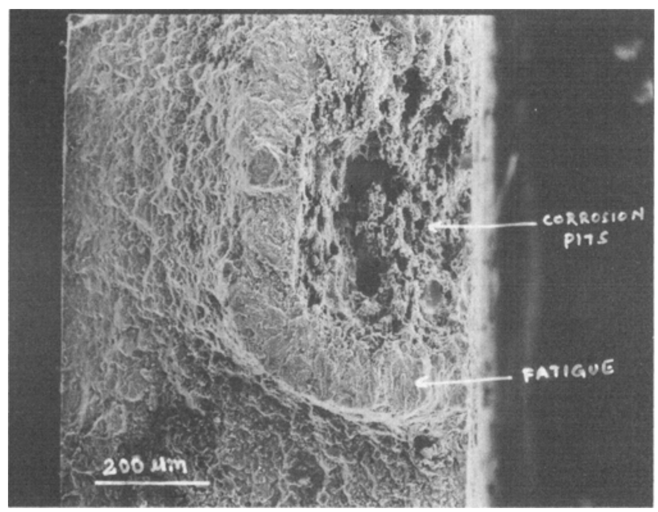

Fig. 19 Scanning electron micrograph of the same specimen in Fig. 18, showing secondary corrosion pitting followed by fatigue cracking

(Fig. 20). Corrosion pits about 0.23 mm (0.009 in.) deep were observed on the specimen surface. For conditions of 30 days precorrosion and $K_t = 3$, secondary cracks were observed on the specimen surface of the 6013 bare alloy, in addition to intergranular cracking and corrosion pits with a depth of 0.28 mm (0.011 in.) (Fig. 21). On the other hand, no intergranular cracking was observed on the fracture surface of the 2024 bare alloy specimens with $K_t = 3$ and both 4 and 30 days of precorrosion; the corrosion pits were 0.19 and 0.30 mm (0.0075 and 0.012 in.) deep, respectively (Fig. 22 and 23). Corrosion pitting increased with longer precorrosion times.

4. Conclusions

The 2024-T3 bare alloy showed better corrosion-fatigue resistance in all cases, with the exception of $K_t = 3$ and 30 days of precorrosion. Visual examination indicated that the surface corrosion in the 2024 alloy was clearly visible and therefore easily inspected. The severity of the surface corrosion increased with precorrosion time. The surface corrosion in the 6013-T6 bare alloy was not clearly visible, and severity increased only moderately.

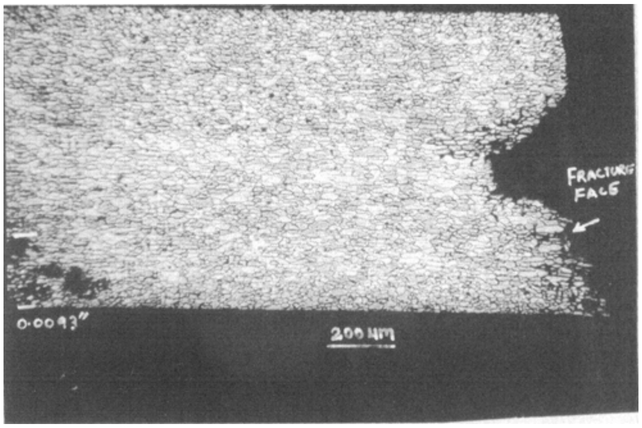

Fig. 20 Optical micrograph of the 6013 bare specimen ($K_t = 3$ and 4 days of precorrosion), showing a corrosion pit with a depth of 0.23 mm (0.009 in.)

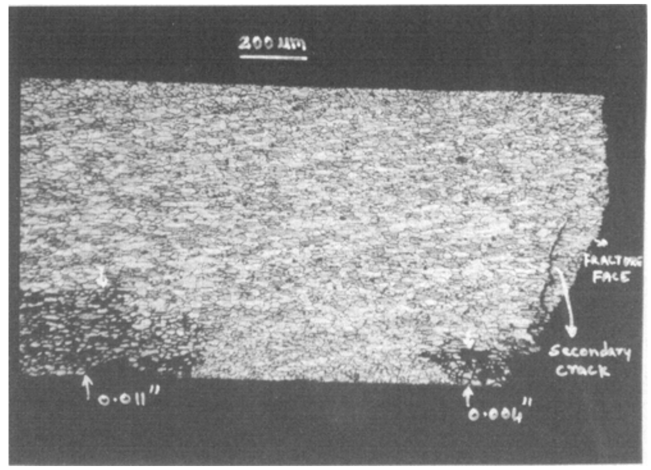

Fig. 22 Optical micrograph of the 2024 bare specimen ($K_t = 3$ and 4 days of precorrosion), showing corrosion pits with a depth of 0.19 mm (0.0075 in.)

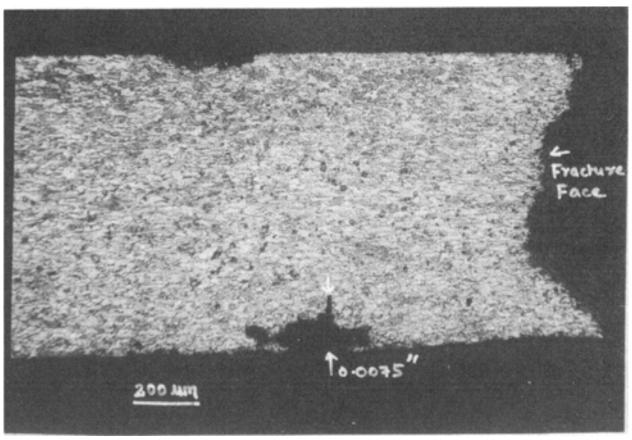

Fig. 21 Optical micrograph of the 6013 bare specimen ($K_t = 3$ and 30 days of precorrosion), showing corrosion pits with a maximum depth of 0.28 mm (0.011 in.) and the presence of a secondary crack

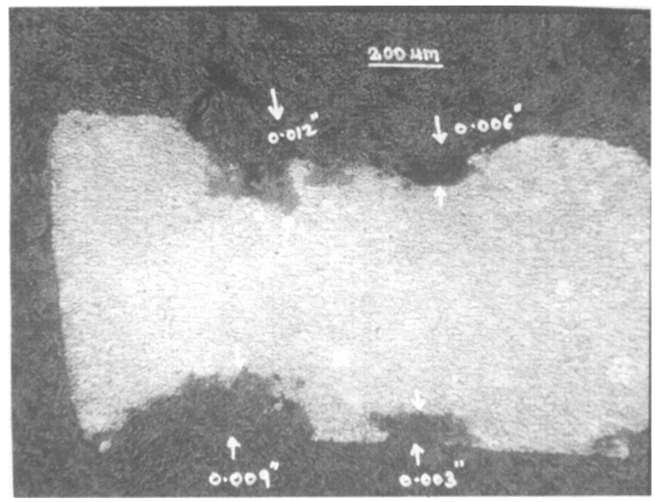

Fig. 23 Optical micrograph of the 2024 bare specimen ($K_t = 3$ and 30 days of precorrosion), showing corrosion pits with a maximum depth of 0.30 mm (0.012 in.)

Fractographic and metallographic examinations demonstrated that only corrosion pits were present near the notch and the surface edge in the 2024 specimens. On the other hand, in addition to corrosion pits, intergranular corrosion cracking was observed in the 6013 bare alloy. Earlier work has shown that the dry-air fatigue lives of the two alloys are comparable. Comparative lower corrosion-fatigue life of the 6013 bare alloy could be due to the intergranular corrosion.

Future work should be directed toward investigation of corrosion-preventive coatings and techniques to improve the corrosion-fatigue resistance of these alloys. In addition, the corrosion-fatigue resistance of other currently used aircraft skin materials, such as 7075 and 7475 aluminum alloys, and potential materials, such as aluminum-lithium alloys, should be explored.

Acknowledgment

J. Chaudhuri and Y.M. Tan wish to acknowledge a grant from the Cessna Aircraft Company.

References

1. S.J. Cieslak, "Alcoa Aluminum Alloy 6013," Alcoa Green Letter 225, 1987, p 23
2. *MIL Handbook 5, Rev. F,* 1990, p 3-108
3. J. Chaudhuri, Y.M. Tan, K.M. Patni, and A. Eftekhari, Comparison of Corrosion-Fatigue Properties of 6013 Bare, Alclad 2024 and 2024 Bare Aluminum Alloy Sheet Materials, *J. Mater. Eng. Perform.,* Vol 1 (No. 1), 1992, p 91
4. J. Mavec, "Metal Bond and Corrosion Characteristics of 6013 Aluminum Alloy," M & P Report No. 84-14-424, Cessna Aircraft Co., 1984
5. K.M. Patni, "Corrosion Fatigue Evaluation Test Plan, 6013 Aluminum Alloy," M & P Report No. 90-87-017, Cessna Aircraft Co., 1990
6. Corrosion Fatigue Failures, in *Metals Handbook,* Vol 9, 9th ed., American Society for Metals, 1985, p 252-262
7. K. Patni, "On the Combined Effects of Bending Stresses and Corrosion on Fatigue Crack Growth," M.S. thesis, 1980, University of Wisconsin—Milwaukee, p 25-27